Available online at www.sciencedirect.com
SCIENCE DIRECT
ELSEVIER
European Journal of Mechanics B/Fluids 24 (2005) 71–90
EUROPEAN JOURNAL OF MECHANICS B/FLUIDS

On the slumping of high Reynolds number gravity currents in two-dimensional and axisymmetric configurations

M. Ungarish *, T. Zemach

Computer Science Department, Technion – Israel Institute of Technology, Haifa 32000, Israel

Received 8 May 2003; accepted 27 May 2004

Available online 28 July 2004

Abstract

The behaviour of an inviscid gravity current of finite volume which is released from behind a lock and then propagates over a horizontal boundary is considered, for the elucidation of the initial 'slumping' phase during which the nose propagates with a constant velocity. The shallow-water two-layer model is used and the necessary front condition is provided, for comparisons, by four different correlations for the nose Froude function. Analytical and numerical results are presented, which reveal the essential flow-field features for various values of the governing dimensionless parameter H, the initial depth ratio of the outer embedding fluid to that of the dense fluid in the lock. It is shown that in the two-dimensional configuration a clear-cut slumping stage develops for any value of H, but for $H < 2$ this stage is complicated by jumps of the interface (backward and forward moving bores) and constrained maximal nose velocity. The two-layer model provides good qualitative and quantitative agreements with previously published measurements, but the one-layer model mispredicts the dependency of the slumping distance on H. In the axisymmetric configuration a clear-cut slumping stage develops only for values of H close to 1 (shallow ambient), and persists for a relatively short time and distance. The effect of the Froude correlations and implementation to box-model approximations are also discussed.

Keywords: Gravity current; Shallow-water equations; Slumping; Front condition; Bore

1. Introduction

The classical gravity current problem considers a rectangular configuration of two incompressible fluids above a horizontal rigid wall at $z = 0$ and bounded by a vertical rigid back-wall at $x = 0$. Initially, the dense fluid of density ρ_d and kinematic viscosity ν fills a reservoir lock of horizontal length x_0 and height h_0, and the less dense ambient fluid, of density ρ_a, fills the remaining volume up to a height H ($\geqslant h_0$). The upper boundary is typically a free surface, and the vertical side-walls are assumed far apart and unimportant to the motion. The gravity current of fixed volume starts to propagate at $t = 0$ in the x direction upon the instantaneous removal of the gate at $x = x_0$. The driving factor is the reduced gravity, defined as

$$g' = \frac{\rho_d - \rho_a}{\rho_a} g. \tag{1.1}$$

We use a two-dimensional Cartesian coordinate system $\{x, z\}$ with the gravitational acceleration g acting in the $-z$ direction. Let h and u denote the height and the longitudinal velocity component of the current; the subscript N denotes the "nose" (front) of the current. It is convenient to scale the dimensional variables (denoted here by asterisks) as follows

* Corresponding author.
E-mail address: unga@cs.technion.ac.il (M. Ungarish).

0997-7546/$ – see front matter
doi:10.1016/j.euromechflu.2004.05.006

$$\{x^*, z^*, h^*, H^*, t^*, u^*\} = \{x_0 x, h_0 z, h_0 h, h_0 H, Tt, Uu\}, \tag{1.2}$$

where

$$U = (h_0 g')^{1/2} \quad \text{and} \quad T = x_0/U. \tag{1.3}$$

Here h_0 and x_0 are the initial dimensional height and length of the current; U is a typical inertial velocity of propagation of the nose of the current, and T is a typical time period for horizontal propagation over a typical distance x_0. We assume a Boussinesq system ($\rho_d/\rho_a \approx 1$), a high Reynolds number ($Re = Uh_0/\nu \gg 1$) and thin layer $h_0/x_0 < 1$, and hence the deformation of the free surface and viscous effects can be neglected and shallow-water approximations can be applied. The advantage of the scaling (1.2), (1.3) is the fact that the aspect ratio of the lock, h_0/x_0, is eliminated from the inviscid shallow-water (SW) analysis which is used here to investigate the behaviour of the current. The scaled problem is specified by one dimensionless number, the geometrical parameter H, which expresses the total dimensionless height of the fluid system, i.e., the ratio of the total height of the ambient to the initial height of the current (lock). It is sometimes more convenient to use $1/H$, referred to as the "fractional depth". This implies an important physical similarity between currents released from a rectangular lock, which is consistent with the experimental observation considered here. (On the other hand, the specification of the aspect ratio h_0/x_0 may be necessary, and may play an important role, in cases where additional accuracy or different similarity laws are of interest, e.g., the numerical solution of the full equations of motion, viscously dominated, particle driven and non-hydrostatic currents. These cases are outside the scope of the present work.)

There is ample experimental evidence that a rectangular gravity current of prescribed volume, released from behind a lock, propagates initially with constant velocity (Keulegan [1], Huppert and Simpson [2], Rottman and Simpson [3]), even in the presence of a stratified ambient (Maxworthy et al. [4]). Following Huppert and Simpson [2] we call this constant-velocity regime the "slumping" stage, and denote the time and distance for which this regime holds by t_s and x_s. The understanding and accurate prediction of the slumping stage behaviour is important from both academic and practical aspects. This is a fundamental ingredient in the development of the motion in most experimental devices and a stringent test for theoretical predictive tools. Some previous investigations of the slumping were presented.

Huppert and Simpson [2] attempted an interpretation of this phenomenon with the aid of a box model, which depicts the two-dimensional current as a spreading rectangle governed by the propagation of the nose based on a specially-derived Froude number correlation (2.12). This is, actually, only a tentative approximation which will be reconsidered in Section 5.

Rottman and Simpson [3] focused considerable attention on the slumping behaviour. They used experimental observations to explain that the extent of the slumping stage is determined by the backward–forward propagation, inside the dense fluid volume, of the depression perturbation created at $x = 1$, $t = 0^+$ by the removal of the lock. They noticed that the nose moves with constant velocity until the depression wave (which first moves from the lock at $x = 1$ towards the wall $x = 0$ and is then reflected) reaches the forward-moving nose. For shallow-ambient currents ($H < 2$, say) an interesting change was noticed: the backward wave concentrates into a jump on the interface which is also reflected as a "bore". Rottman and Simpson [3] plotted the measured x_s as a function of the initial fractional depth $1/H$ (Fig. 11 in that paper), to show that x_s displays significant decrease, from about 10 to 4, when H changes from 1 to 10.

The theoretical attempts to recover and explain the slumping observations by analytical or numerical simulations of the SW equations yielded partial success. The deficiencies of the available theoretical coverage of the slumping behaviour are most pronounced for the configurations with $H < 2$, where left- and right-moving bores appear and the measured slumping distance increases dramatically (as compared to the $H > 2$ counterparts). The reasons are as follows.

The simplest and generally used SW formulation is the one-layer model which assumes a hydrostatic ambient and is therefore accurate only for a very deep ambient configuration, $H \to \infty$. However, this model is also used as an approximation for non-deep ambients, i.e., finite and not necessarily large values of H. This model predicts that the initial propagation is with constant velocity for any $H \geqslant 1$, but, as shown later in Section 3.1, the details of the predicted slumping distance x_s deviate considerably from the physical observations when H is not very large. The more accurate two-layer SW formulation was used by Rottman and Simpson [3]. They obtained numerical solutions by the method of characteristics, but that numerical method provided valid results only for $H > 2$. For $H < 2$ a singular behaviour of the interface was detected, but not resolved. Moreover, the results presented by [3] for $H = 1$ (Fig. 7(c) in that paper) indicate that their solution overlooks the critical velocity constraint (i.e., the front of the current cannot propagate faster than the characteristic moving in the same direction) and therefore even the front velocity results are physically unacceptable for H close to 1 (this issue will be elaborated in Section 2.3.1). Consequently, the paper [3] could not provide a two-layer SW analysis to the slumping behaviour for $H < 2$ (and even for $H > 2$ this paper presents only a very brief theoretical discussion of the slumping phase). Klemp et al. [5], using the two-layer SW formulation, showed analytically that for $H < 2$ the backward-moving depression wave produces a "jump" at the interface, and developed the necessary matching conditions, see below. They presented a detailed analytical description of the initial motion of the nose using the Froude relationship of Benjamin [6], subject to the critical velocity constraint. However, this study assumed a semi-infinite reservoir of dense fluid, $-\infty < x \leqslant 1$ and therefore could not detect the essential influence of the wall at $x = 0$

on the slumping of a realistic finite-volume current. In other words, this study does not capture the reflection of the jump (or depression wave) as a forward-moving bore (or wave), and therefore $x_s = \infty$ in the investigated configuration. Bonnecaze et al. [7] used a Lax–Wendroff finite difference method to solve the two-layer SW formulation used by Rottman and Simpson [3], and obtained also results for the $H = 1$ case. However, in this numerical solution the jump at the interface was implicitly smoothed by artificial viscosity, and no attention has been focused on the prediction of the initial slumping behaviour. D'Allesio et al. [8] solved the two-layer equations by MacCormack's method, using uspecified boundary conditions on the nose and artificial viscosity. Again, the slumping behaviour has not been discussed, but indirect results indicate significant exaggerations of the calculated x_s (e.g. Fig. 9 in that paper suggests $x_s = 14$ for $H = 1.11$ which is about 40% above the measurements of [3]). No SW investigations for the slumping phenomenon in the axisymmetric configurations were presented, to our best knowledge.

It has been recently pointed out that slumping occurs also in circumstances of stratified ambient fluid (Maxworthy et al. [4], Ungarish and Huppert [9]). Some recent investigation of non-classical effects in gravity current propagation (e.g. Coriolis and particle settling, see [10]) are based on perturbations about the self-similarity solution, and the evaluation of errors contributed by the previous slumping stage becomes of critical importance to the applicability of theses results. There are experimental indications that the slumping delays entrainment, see [11]. However, the slumping distances needed in these and similar studies were estimated by ad-hoc correlations and interpretation of experimental data rather than from firm analytical knowledge. Indeed, in spite of its wide and significant manifestation, the slumping phenomenon lacks a comprehensive definitive theoretical study. Consequently, one may find in the literature confusing and even misleading statements about slumping. Moreover, the dependency of the slumping behaviour on the geometry (e.g., axially symmetric vs. rectangular) has not been established. The need for more knowledge about this phenomenon motivated the present study.

The present work is an extension of the studies of Rottman and Simpson [3] and Klemp et al. [5]. The objective is to clarify further the slumping behaviour of a gravity current of finite volume. We use analytical and numerical solutions of one- and two-layer SW formulations. Our numerical code for the two-layer model is similar to that used by [7], but specially designed to cover accurately (using analytical jump conditions) the velocity and amplitude of the left-moving discontinuity at the interface in the problematic range $1 \leqslant H \leqslant 2$. Four different formulas for the nose Froude number correlations with h_N/H were used in order to asses the effect of this closure on the slumping behaviour. Furthermore, the axially-symmetric case is also considered.

The structure of the paper is as follows. The formulation of the SW model and some consequences regarding essential features of the slumping phase (e.g., jumps at the interface and constrained nose velocity) are presented in Section 2. Analytical and numerical results for the rectangular 2D case are discussed and compared with available experimental data in Section 3, and a brief extension to the axisymmetric case is given in the next section. In Section 5 the implications of the present results on box-model approximations is discussed. Finally, in Section 6 some concluding remarks are presented.

2. Formulation

We use the shallow-water two-layer inviscid model. The layer of dense fluid is in $0 < x < x_N(t)$ and $z < h(x,t)$. As the current passes over the bottom, a return flow is set up within the ambient above as a consequence of volume continuity, and it is assumed that there is no interfacial drag between the two layers and the upper boundary is a frictionless horizontal wall (rigid lid). The flows in both layers are represented by z-averaged equations. We will discuss in detail the rectangular case, and extensions to axisymmetric configurations are considered in Section 4.

2.1. The governing equations

The equations of motion were formulated by Rottman and Simpson [3] for the ambient (upper) and current (lower) layers. By eliminating the pressure from the momentum equations for each layer, these equations can be reduced to a system of two PDEs which contains only the lower-layer variables h and u. The resulting shallow-water equations can be expressed in dimensionless form for the lower layer variables by

$$\begin{cases} \dfrac{\partial h}{\partial t} + h\dfrac{\partial u}{\partial x} + u\dfrac{\partial h}{\partial x} = 0, \\ \dfrac{\partial u}{\partial t} + (1-2a)u\dfrac{\partial u}{\partial x} + (1-b)\dfrac{\partial h}{\partial x} = 0, \end{cases} \tag{2.4}$$

where

$$a = \frac{h}{H-h} \quad \text{and} \quad b = \frac{h}{H} + \frac{u^2}{H}\left(1 - \frac{h}{H}\right)^{-2}. \tag{2.5}$$

The equations represent conservation of volume and horizontal momentum in the dense fluid layer (the term $\partial h/\partial x$ reproduces the pressure gradient). The equations are valid in the domain $0 \leqslant x \leqslant x_N(t)$, where $x_N(t)$ is the dimensionless position of the nose.

The equations that connect between the upper- and lower layers are:

$$\begin{cases} h_u = H - h, \\ u_u = -\dfrac{uh}{h_u}, \end{cases} \tag{2.6}$$

where h_u and u_u are the height and the velocity of the upper layer of ambient fluid.

In the limit $H \to \infty$ the two-layer equations (2.4)–(2.6) reduce to the one-layer model governing equations, as discussed later.

2.2. The characteristics

The characteristic paths and relationships provide useful information for the solution of the (presumed) hyperbolic system (2.4), including a proper definition of boundary conditions for the interface height h at the ends of the current domain.

The characteristic velocities (assumed real and distinct) are

$$c_\pm = u(1-a) \pm \sqrt{(au)^2 + (1-b)h}, \tag{2.7}$$

and the relationships between the dependent variables on the characteristics with $\mathrm{d}x/\mathrm{d}t = c_\pm$, can be expressed as

$$\frac{\mathrm{d}h}{\mathrm{d}u} = \frac{1}{1-b}\left[au \mp \sqrt{(au)^2 + (1-b)h}\right]. \tag{2.8}$$

Both (2.7), (2.8) contain a complex dependency on H. An inspection of this dependency (with some hindsight) shows that, in general, the two-layer system displays an increasing "rigidity" as H decreases towards 1, in the sense that the propagation of initial perturbation becomes slower and encounters more opposition when the gap between the (inviscid) bottom and top walls of the tank is reduced for a given height of the lock. This feature is, as expected, very pronounced for $H < 2$ because the lower current must induce an even stronger flow in the upper layer. The slumping behaviour is dominated by the propagation of these initial perturbation. This creates qualitative differences in the shape of the interface between the $H > 2$ ("deep ambient") and $H < 2$ ("shallow ambient") cases, and, for $H < 1.25$ (approximately) the matching conditions at the nose are also affected. The details are discussed below.

2.3. The nose velocity

The boundary condition for the velocity at the nose is essential for a proper physical definition and mathematical closure of the problem. The consensus it that the nose of a "real" time and space dependent gravity current obeys a local, quasi-steady-state correlation between velocity and height, that is essentially similar with the theoretical results obtained for idealized infinite systems by Benjamin [6],

$$u_N = Fr\, h_N^{1/2}, \tag{2.9}$$

where the Froude 'number' Fr varies in a limited range about the value of unity, and is actually a decreasing function of (h_N/H) only.

Experiments confirmed this qualitative behaviour, but also indicated that the theoretical value of Fr, derived by Benjamin [6] for a highly idealized motion, over-predicts (by typically 20%) the velocity in real circumstances. To reconcile theory with practice, several simple modifications have been suggested. In the present work we use, for comparison, the following four correlations.

(1) The theoretical formula of Benjamin [6], referred to as B,

$$Fr(\alpha_N) = \left[\frac{(2-\alpha_N)(1-\alpha_N)}{1+\alpha_N}\right]^{1/2}, \tag{2.10}$$

where $\alpha_N = h_N/H$.

(2) Rottman and Simpson [3] suggested the correlation, referred to as RS,

$$Fr(\alpha_N) = \frac{1}{\sqrt{2}}\left[\frac{(2-\alpha_N)(1-\alpha_N)}{1+\alpha_N}\right]^{1/2} \tag{2.11}$$

to improve the agreement between their SW results and experiments.

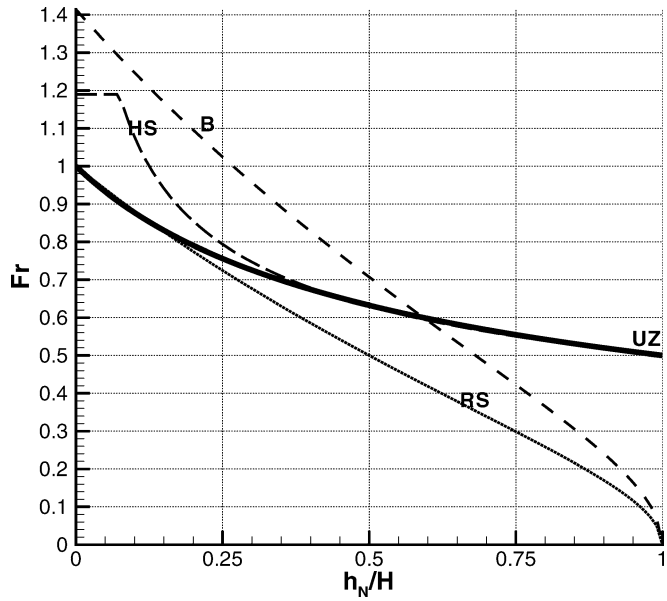

Fig. 1. The Froude number correlations.

(3) Huppert and Simpson [2] developed the well-known curve-fit type correlation, referred to as HS,

$$Fr(\alpha_N) = \begin{cases} 1.19 & (0 \leqslant \alpha_N \leqslant 0.075), \\ 0.5\alpha_N^{-1/3} & (0.075 \leqslant \alpha_N \leqslant 1). \end{cases} \tag{2.12}$$

This formula is of special interest in the present study, because it has been presented by Huppert and Simpson [2] as an essential part of their slumping model, as discussed in Section 5. Unless stated otherwise, this correlation is used for the numerical results presented in our paper.

(4) The forth correlation, referred to as UZ, is suggested here for the first time,

$$Fr(\alpha_N) = (1 + 3\alpha_N)^{-1/2} \tag{2.13}$$

and is a semi-empirical and simplified "compromise" between the foregoing correlations, weighted in favor of (2.11) for small values of h_N/H, in accordance with experimental observations.

These functions are plotted in Fig. 1. The notable difference is for h_N/H close to 1: the first two correlations tend to the value 0, while the last two tend to the value 0.5. From the viewpoint of the SW theory this is unimportant, because solutions with h_N larger than about 0.6 do not occur, but the box model discussed in Section 5 uses this information when $H < 2$.

The deviations from the theoretical Fr appear because in real gravity currents various departures from the idealized model are unavoidable, such as: the complex three-dimensional structure of the head, time dependency, turbulent mixing, entrainment, friction, etc. It is therefore unlikely that a perfect, generally accurate one-parameter fit can be obtained, but a prototype correlation closure is necessary for progress. It will become evident that the essence of the analysis and conclusions are not affected by small details of the functional form of $Fr(h_N/H)$. The particular correlation affects the quantitative value of u_N during the slumping stage, and the extent of this stage, but the appearance of the slumping and the main subsequent time-dependent behaviour remain unchanged.

2.3.1. "Critical" nose region for $H < 1.25$

We notice that the value $b = 1$ indicates a "critical" change of behavior for the forward-moving characteristics: (2.7) predicts that $c_+ > u$ for $b < 1$, and $c_+ < u$ for $b > 1$. (Also, at $b = 1$ we obtain a singular behaviour of $\mathrm{d}h/\mathrm{d}u$ on the c_- characteristic.) As discussed by [6] and [5], due to stability and maximum dissipation consideration, in practical lock-release problems the nose, treated as a shock discontinuity, cannot (rather, it usually does not) travel faster than the fastest characteristic in the adjacent dense fluid. The detailed numerical solution of a lock exchange gravity current over a no-slip boundary, based on the Navier–Stokes equations for a Boussinesq fluid, also supports this velocity limitation, see [12]. Following these considerations and evidence we incorporate this condition in our model and we shall show later that it provides useful qualitative interpretations

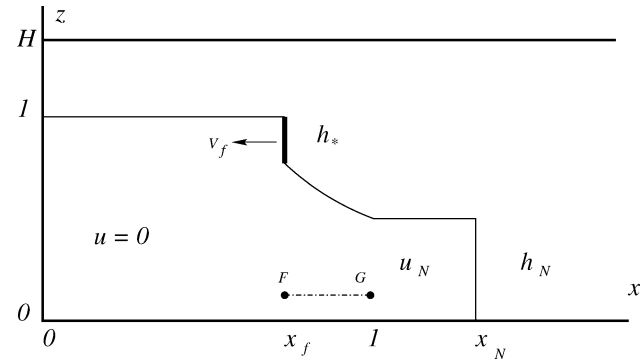

Fig. 2. Schematic description of a two-layer current during the initial slumping stage in the $H < 2$ case (shallow ambient configuration), showing the left-moving jump at the interface (thick line). (The constant u and h rectangular region $x > 1$ behind the nose appears when sub-critical matching is feasible. When the critical constraint $u_N = u_{N\max}$ is relevant, the rectangular region behind the nose is modified: the interface is slightly downwardly-inclined, and u increases with x.)

and accurate quantitative predictions of observed slumping motions. Thus, the condition $b \leqslant 1$ at the nose imposes an upper limit constraint, or choke, on the velocity of the nose

$$u_N < u_{N\max} = \left[H(1 - h_N/H)^3\right]^{1/2} \tag{2.14}$$

for given H and h_N.

In general it is necessary to subject the nose velocity in the subsequent calculations to (2.14). However, an estimate based on the typical $h_N \approx 0.5$ shows that $u_{N\max} > 0.9$ for $H > 2$, and hence this formal restriction is straightforwardly satisfied by gravity currents in a non-shallow ambient; in these cases $b < 1$ in the entire current. Actually, (2.14) requires special attention only for $H < 1.25$ approximately; in these cases, a domain with $b > 1$ appears behind the nose.

2.4. Jumps of interface for $H < 2$

2.4.1. Left-moving discontinuity

The numerical solution of Rottman and Simpson [3] indicated that for $H < 2$ a singularity appears in the profile of the interface behind the lock. The analysis of this effect, presented by [5], reveals the following features. Upon the release of the lock, a depression perturbation propagates back with velocity c_- into the still motionless body of dense fluid. Note that $|\mathrm{d}c_-|/\mathrm{d}h$ is positive for $H > 2h \approx 2$, and negative for $H < 2h$. Thus, for $H > 2$ the leading edge of the depression wave (where $h = 1$) travels faster than the trailing portions (where $h < 1$) and the depression spreads with time. However, for $H < 2$, the trailing portions of the wave propagate faster than the leading edge and thus the depressed interface continues to steepen until it forms a discontinuity (jump). This discontinuity reaches quickly a steady height h_* and speed V_f (to the left), see Fig. 2 (which prevail until the jump attains the end-wall $x = 0$). Klemp et al. [5] showed that the pressure and force balances, when dissipation is neglected, yield

$$V_f^2 = \frac{\gamma^2 - \alpha^2}{(2\gamma^2 - \alpha)/\alpha + [(1-\gamma)/(1-\alpha)]^2(1-2\alpha)} \cdot \frac{1}{\gamma} \quad (H \leqslant 2), \tag{2.15}$$

where $\gamma = 1/H$ and $\alpha = (1 - h_*)/H$. Due to continuity the velocity of the dense fluid below and to the right of the jump is, obviously, $u = h_* V_f/(1-h_*)$. The additional condition for this steady-state jump is provided by the Stommel and Farmer [13] constraint (derived by an analysis of the general properties of the SW two-layer solutions),

$$\frac{(u + V_f)^2}{1 - h_*} + \frac{(u_u + V_f)^2}{h_u} = 1, \tag{2.16}$$

applied to the domain on the right side of the discontinuity. The combination of (2.15), (2.16), supplemented by the connection (2.6) between the upper and lower layer variables, provides unique results for h_* and V_f, as depicted in Fig. 3. Fitted approximations are given in Appendix B. The left-moving front becomes similar to the right-moving nose in the limit $H \to 1$. In this case $h_* = 0.347$ and $V_f = 0.528$ which indeed are the counterpart of the propagation of a gravity current in a configuration with $H = 1$ and the idealised Fr of Benjamin (2.10) subject to the "critical" condition $b = 1$. However, there is experimental and theoretical support (see discussion in [5]) to the assumption that the left-moving front is unaffected by dissipation. The upper discontinuity is not in touch with a solid boundary and therefore is less exposed to viscous influence than the nose which

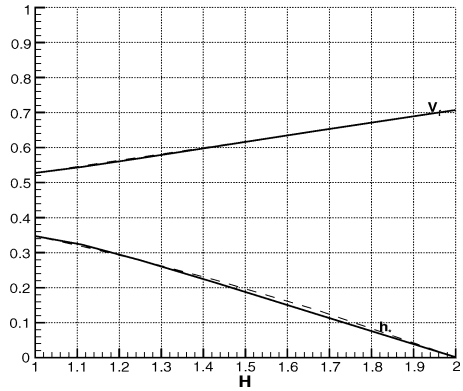

Fig. 3. Speed V_f and the height h_* of the left-moving jump (solid lines) and the curve-fit approximations (dashed lines).

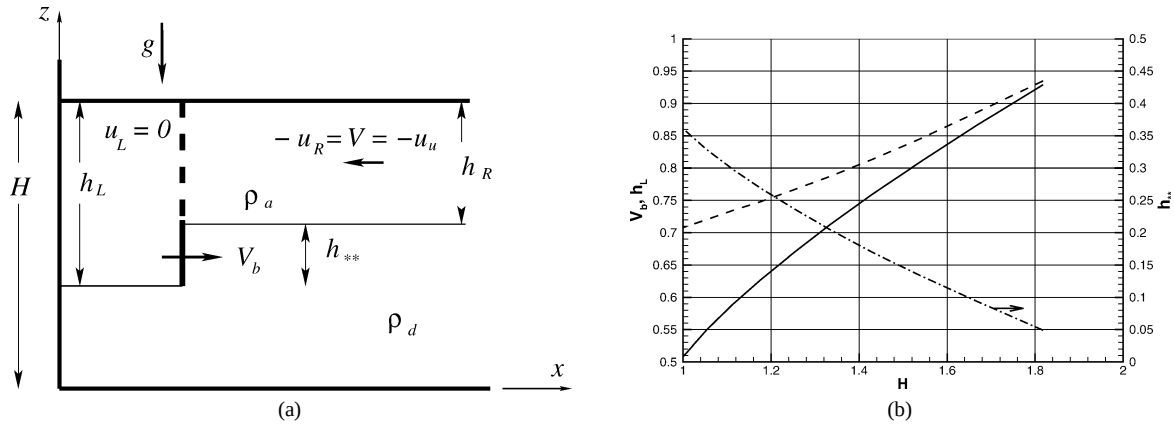

Fig. 4. The bore (a) simplified configuration; (b) speed (solid line), height (dashed line), and height of penetration into the lower layer (dash–dot line) as functions of H.

moves above the bottom. These considerations justify the use of the idealized calculation of V_f even for situations where the nose is governed by the empirically-adjusted *Fr*.

2.4.2. The reflected bore

At $t = t_f = 1/V_f$ the left-moving discontinuity hits the wall at $x = 0$. The upper-layer fluid in the region $x > 0$ has a considerable negative velocity at this time and hence the impingement on the wall forms immediately a shock-wave (bore, hydraulic jump), that propagates into the fluid. (The related "moving wall" problem is discussed by [14, §8.1.2].) The absolute velocity of the bore is V_b, and the region of fluid left behind has a typical deep penetration into the adjacent layer of fluid. This is consistent with the observations of [3].

A simplified analysis of this phenomenon is developed here using the configuration sketched in Fig. 4.

The jump conditions across the shock are assumed to be, in the frame of reference of the shock, conservation of volume and of $u^2h + (1/2)g'h^2$ (dimensional). In the absolute $x - z$ laboratory system, at the left side of the shock (near the wall) there is a region of zero velocity and (unknown) thickness h_L, and at the right side there is the upper-layer fluid, whose velocity $u_u = -V$ and $h_u = h_R$ are known from the solution of (2.15), (2.16).

After some algebra, we obtain equations for the shock velocity and height of the quiescent region behind the shock in dimensionless form, as follows

$$V_b = \frac{V}{\chi - 1}, \tag{2.17}$$

$$(1-\chi)^2(1+\chi) - 2\frac{V^2}{h_R}\chi = 0, \tag{2.18}$$

where

$$\chi = \frac{h_L}{h_R}. \tag{2.19}$$

The solution of (2.18) in the range $\chi > 1$, for given values of V and h_R, is straightforward. The velocity and height of the bore (at the position of formation) as a function of the total depth H are given in Fig. 4. The penetration height, $h_{**} = h_L - h_R$, which represents the strength of this shock, decays to zero as H approaches 2, as expected. We notice that when H increases from 1 to 2, V_b increases by a factor 2, roughly. This explains the quite drastic decrease of the slumping distance in this range of H. Since the velocity of the nose increases only slightly with H, see Fig. 8, the relative velocity between the bore and the nose increases strongly with H.

The rate of dissipation of energy across the shock can also be calculated, see [14], but this topic is left open for future study. It is well known that various sets of assumptions can be applied to derive the propagation of hydraulic jumps, [15], and careful revisions are necessary to establish the most appropriate choice on account of available experimental evidence. Such an investigation was performed recently by [16] using the experimental data of [17] and others, but the considered configurations are apparently different from ours. We hope that eventually more experimental data will become available to allow a similarly thorough investigation and improvement of the present tentative theory. In any case, the results provided by the suggested model are consistent with the presently available experimental and numerical data, so it makes sense to employ this approximation in spite of doubts about the validity of the underlying assumptions.

In the real configuration the velocity field in the upper layer is x-dependent. This suggest a straightforward modification of the present model upon using the local values $V(x)$ and $h_R(x)$ in (2.17), (2.18). The quantitative details are complicated because the flow-field changes with time, but the qualitative behaviour can be estimated under the assumption that the time variations prior to the arrival of the bore are small, i.e., the flow is "frozen" at the time t_f. Using the results developed in Section 3 we find a mild increase of V_b and of h_{**} with time. This, again, is consistent with the numerical solution of the SW model. Rottman and Simpson [3] claim that the experimental velocity of the bore is constant, but the theoretical variation of V_b is sufficiently small for being in the range of the experimental uncertainties.

The present analysis of the bore omits the contribution of the lower layer of fluid to this effect. The heuristic justifications are: (a) The lower layer is taken into account implicitly in the right side of the shock, because we use the values of V and h_R that are provided by the two-layer model solutions. (b) The velocity u in the fluid below the left side of the shock is expected to be small near $x = 0$, anyhow, and hence the effect of this layer is small, at least during the time when the bore is created. The fair agreement with experimental and numerical data, as discussed in Section 3.2, vindicates these approximations.

An analytical estimate of the slumping time and distance can be obtained under the assumption that V_b is constant,

$$t_s = t_f + t_b = \frac{1}{V_f} + \frac{1 + u_N/V_f}{V_b - u_N}, \qquad x_s = 1 + t_s u_N, \tag{2.20}$$

where t_b is the time of propagation of the bore to the nose. This can be considered an upper bound because the expected increase of V_b with time. For $H = 1$ and the HS Fr correlation we obtain $t_s = 24.5$ and $x_s = 11.6$ (which is 9% above the experimental value of [3]). In this case the theoretical $u_N = u_{N\max} = 0.43$.

Comparisons with numerical solutions of the SW equations and with the experimental results presented in Fig. 8 of [3], as discussed later, show fair agreement with the present approximations. We therefore infer that the simple model developed here captures well the essential features of the reflected bore.

2.4.3. Boundary conditions

The initial conditions for the dense fluid are $u = 0$, $h = 1$ and $x_N = 1$. Following the foregoing discussion, we conclude that for $H \geqslant 2$ the boundary conditions can be provided straightforwardly at the left boundary $x = 0$ and at the nose $x = x_N(t)$. For $H < 2$ the left boundary of the domain of solution, and the conditions there, are dictated by the presence and position of the left-moving discontinuity. For $H < 1.25$ (approximately) the nose velocity is still related to $h_N^{1/2}$ by the Froude number condition (2.9), but reaches the $u_{N\max}$ value (which cannot exceed the c_+ characteristics from the trailing fluid). In this case the value of h_N is determined by the intersection of (2.9) and (2.14).

2.5. Method of solution

The foregoing SW formulation is a closed hyperbolic system of PDEs for the variables $h(x,t)$ and $u(x,t)$ in the cases considered in this work. In general, the calculation of these variables requires a numerical solution, which is complicated by the fact that the domain varies with time, the boundary conditions of h are not known explicitly, and the problem is not necessarily well-posed. We use a two-step Lax–Wendroff finite difference scheme. The physical spatial domain of interest is first mapped into a computational domain of constant length, $0 \leqslant y \leqslant 1$, which is discretized into a constant number of intervals, typically 200. For $H \geqslant 2$ the left boundary of the domain is fixed at $x = 0$. For $H < 2$ a more complicated code is necessary, to account for the moving discontinuity at the left boundary and the constrained velocity of the nose. The boundary conditions

of h, when unspecified, are calculated, each time step, from the balance on the characteristics which reach the needed points. This turns out to be an efficient and versatile approach. The details of this numerical approach are given in Appendix A.

However, useful insights and even some quantitative results can be obtained from simplified considerations of local balances, in particular during the initial stages of the slumping motion. We call this approach "analytical" (but, in the strict sense, it also involves numerical tools for the solution of non-linear equations and integration of ODEs).

The following discussion is based on a combination of these analytical and numerical approaches.

3. Results

The values of h_N and u_N during the slumping phase and the essential geometry of the fluid domain following the nose can be predicted analytically. It is convenient to consider first the one-layer limiting case.

3.1. The $H \to \infty$ limit and one-layer SW model

For $H \to \infty$ the governing equations (2.4) and the characteristics (2.7), (2.8) are drastically simplified by the fact that $a = 0$ and $b = 0$ in this limit. Motion takes place only in the layer of the dense fluid, and a purely hydrostatic balance prevails in the ambient fluid domain. In this respect, the widely used one-layer SW model, which is developed under the assumption that the ambient is motionless, is recovered. For consistency, in the $H \to \infty$ limit $\alpha_N = 0$ should be used in the Fr correlations (2.10)–(2.13). However, the one-layer SW model is commonly employed also as an approximation to the two-layer flow for finite values of H, as follows: the equations of motion obtained for $H \to \infty$ are solved, but the finite value of H is kept in the Fr correlation for the nose boundary condition (2.9). It is natural to ask if, and with what accuracy, can the slumping phase be predicted by this model.

We find that the SW one-layer model, for both the consistent $H \to \infty$ and finite H nose condition, yields an initial slumping stage of propagation with constant velocity u_N and, accordingly, with constant h_N (the values of u_N and h_N depend on the Fr correlation and on H). Moreover, in the corresponding time period the moving nose is followed by a rectangular domain of constant height and velocity, as sketched in Fig. 5. This behaviour in the region following the nose is indicated by the fact that (2.8) admits a non-trivial solution with $\mathrm{d}h = \mathrm{d}u = 0$, and has been confirmed by numerical solutions of the SW equations.

Consider the current fluid domain sketched in Fig. 5. The values of h_N and u_N during the slumping phase can be predicted analytically by the dam-break problem methodology, following a forward-propagating characteristic c_+ from a point F in the still unperturbed domain where $u = 0$ and $h = 1$ to a point G in the domain where the velocity and the height have the constant values u_N and h_N. The connection between the variables at these points is given from integrating (2.8). On the other hand, u_N is given by the boundary condition (2.9) plus one of the correlations (2.10)–(2.13). The intersection of these conditions yields an equation for h_N (with H as parameter),

$$u_N = 2\left(1 - h_N^{1/2}\right) = Fr(h_N) h_N^{1/2}. \tag{3.21}$$

Solutions of (3.21) were obtained for $0 < 1/H \leqslant 1$ for the different functions $Fr(h_N/H)$ considered in this work, as shown if Fig. 6 (the accuracy of the predicted u_N can be inferred with the aid of Fig. 8).

Since $b = 0$ in the one-layer model the nose velocity constraining condition $b_N \leqslant 1$ is inherently satisfied. It is therefore evident that the one-layer model prediction concerning the formation of a slumping stage is quite insensitive to the small details of the behaviour of Fr as a function of h_N/H.

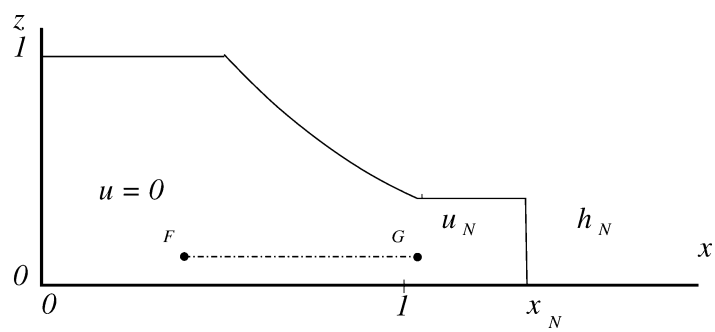

Fig. 5. Schematic description of a one-layer current during the initial slumping stage, $t < 1$. The inclined interface is in the domain $-t < x - 1 < (u_N - \sqrt{h_N})t$ and is given by $h(x,t) = [2 - (x-1)/t]^2/9$.

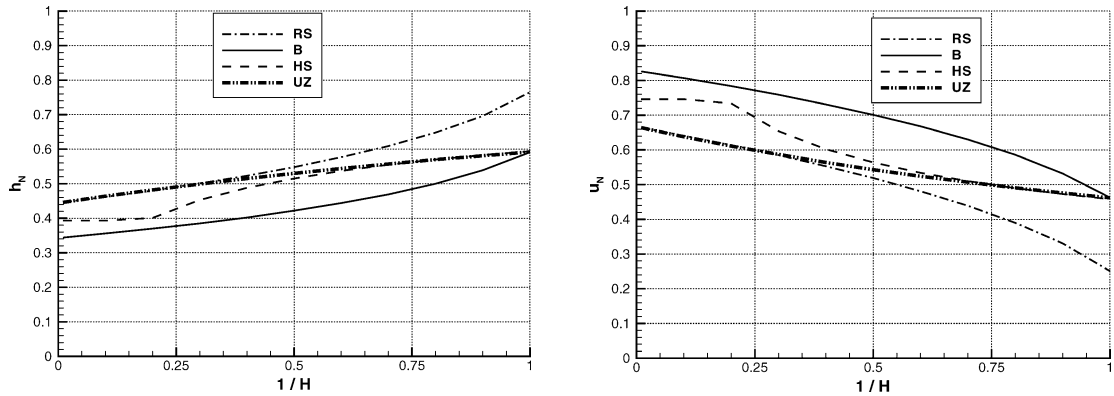

Fig. 6. One-layer model slumping results for h_N and u_N as functions of $1/H$ for various Fr correlations.

The numerical solutions of the SW equations confirm the previous results, and also provide the details of the time-dependent behaviour of the shape of the current. There are essentially two phases during which the speed of propagation is constant. First, while the nose propagates forward, a depression wave propagates backwards, see Fig. 5, until it reaches the endwall $x = 0$ at $t = 1$. This is like in the classical dam-break of a semi-infinite reservoir ($-\infty < x \leqslant 1$). Next, in contrast with the semi-infinite reservoir case, the reflected depression wave propagates from the wall at $x = 0$ towards the nose. The inclined portion of the interface is affected first and eventually (at $t \approx 3$) the entire current is flattened to, approximately, a rectangular profile of height h_N and, by continuity, of length $1/h_N$. The initially-inclined interface (at $x < 1$, approximately) descends further, and this information is propagated forwards, with velocity $u_N + h_N^{1/2}$, into the initially-rectangular domain. The position of the nose when it is reached (and affected) by this wave is given by

$$x_s = \frac{2}{h_N} - 1, \qquad t_s = \frac{x_s - 1}{u_N}. \tag{3.22}$$

Afterwards the height of the nose is bound to decrease, and the constant velocity u_N cannot be sustained anymore.

Substituting the previous results for h_N and u_N (obtained from (3.21) for a specific H and Fr correlation) into (3.22) we obtain, explicitly, the slumping distance and time. The values are in agreement with the numerical solution of the SW time-dependent equations. However, these theoretical x_s agree quantitatively with the experimental observations only for large values of H, for which $x_s \approx 4$ and $t_s \approx 5$ (to be more specific, 4.6, 3.4, 3.9 and 3.4 for the Fr correlations B, RS, HS and UZ, respectively). When H decreases to 1 the experimental x_s (see [3]) increases to about 11, while the one-layer model predicts that x_s decreases monotonically (below the abovementioned values) when H decreases, for all the tested Fr correlation. Thus, the variation of x_s predicted by the one-layer model with H is wrong, and the discrepancies are more that 100% when H approaches 1.

This failure of the one-layer model can be attributed to the fact that the propagation of the perturbations in this approximation is with $c_\pm = u \pm h^{1/2}$, independent of H, while the real two-layer system becomes more and more rigid (the propagation of perturbations is hindered) when H decreases. Keeping the dependency on H in the Fr correlation reduces the velocity of the nose when H decreases, and hence the backward–forward moving perturbations are able to reach the nose in a shorter time, just the opposite from what happens in a real system.

We must recognize that the one-layer formulation used in the two-layer context is an over-simplifications that is inadequate for the prediction of the slumping behaviour (except for $H \to \infty$). We show below that the two-layer model provides the correct features of the slumping phase for all H.

3.2. The general case

As in the one-layer case, we attempt to follow the development of the variables h and u along a forward-propagating characteristic, c_+, starting from a point F with known conditions in the $x < 1$ domain, to a relevant point G (typically, at $x \approx 1$, on a matching c_- characteristic emanated at the lock) in the fluid behind the nose. Using (2.8) we obtain, formally,

$$u_G(h_G; h_F, u_F) = \text{Solve}\left\{\frac{\mathrm{d}u}{\mathrm{d}h} = (1-b)\left[au - \sqrt{(au)^2 + (1-b)h}\right]^{-1}\right\}, \tag{3.23}$$

where a and b are functions of h, u and of the parameter H, and h_F, u_F are prescribed initial conditions. The integration must be performed numerically, e.g. by a Runge–Kutta method. The function on the right-hand side is negative (for $b \neq 1$),

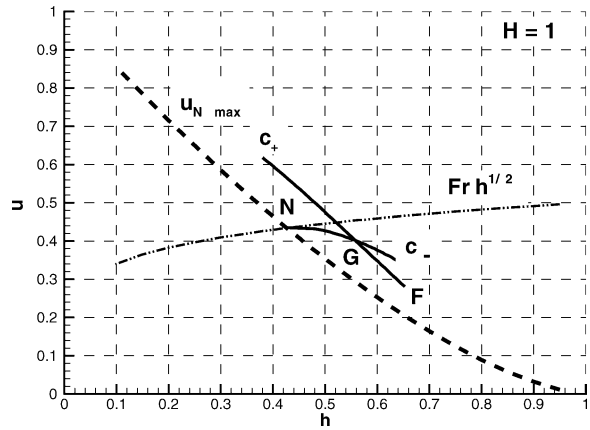

Fig. 7. The characteristics and velocities in the h–u plane for $H = 1$. Point F is below the backward-moving discontinuity, and point N denotes the nose, h and u in the current are given by the path FGN along the characteristics with c_+ and c_-. The HS Froude correlation was used. Note that $b < 1$ on the left side of the $u_{N\max}$ line, and $b > 1$ on the right side.

consistent with the fact that for the initial slumping phase we are interested in a forwardly propagating characteristic along which h decreases and u increases (in the simplest case, from zero to u_N). We note that the value of b increases in the direction of propagation.

Consider a configuration with $H > 2$. In this case the interface $h(x, t)$ is continuous, and points F and G can be conveniently taken like in the one-layer case sketched in Fig. 5, i.e., the integration starts with $h = 1$ and $u = 0$, and ends in the rectangular region of constant height and velocity which trails the nose. Thus, the height and velocity given by (3.23) at point G are intersected with the nose velocity condition (2.9) to obtain h_N and u_N. It turns out that the value of b is always smaller than 1 along the path of integration, and hence the $u_{N\max}$ restriction, see (2.14), is implicitly satisfied.

In a configuration with $H < 2$, point F must be taken at the entry position below the left-moving jump of the interface, see Fig. 2. Since h and u there are known, the previous calculations for h_N and u_N can be repeated. Point G is as above if H is sufficiently large so that $u_G = u_N \leqslant u_{N\max}$ can be attained by direct integration along c_+. Otherwise, the $u_{N\max}$ constraint introduces a different matching conditions between points F and N. This effect has been discussed by Benjamin [6] and Klemp et al. [5] for the *Fr* relationship B, and it turns out here that it can be similarly applied to the other *Fr* correlations considered in this work. Indeed, for $H < 1.25$ (the exact value depends slightly on the specific *Fr* correlation) the value of b in (3.23) may exceed 1, which means that direct matching between the bulk of fluid and the nose along this path would require a non-physical nose velocity larger than $u_{N\max}$. This non-physical situation is avoided with the help of a buffer expansion zone which is allowed to develop between point G (where $b > 1$) and the nose (where $b_N = 1$). In this case the nose propagates with the critical value of $u_{N\max}$ for the corresponding h_N, given simply by the intersection of (2.9) with (2.14). The domain left behind the nose is typically governed by the c_- characteristic, with $\partial h/\partial x < 1$ and $\partial u/\partial x > 1$. (The integration along the c_- characteristic is conveniently performed from the nose backwards, using (2.8).) The diagram in the h–u plane of the characteristics and other velocities, for the case $H = 1$ with the HS nose correlation, is illustrated in Fig. 7. We note in passing that a similar diagram but using the B nose relationship yields the symmetric $h_G = 0.5$ result.

A summary of analytical results obtained by the abovementioned calculations is presented in Fig. 8. It displays the nose velocity u_N and the nose height h_N as functions of $1/H$ for the four suggested functions $Fr(h_N/H)$. For $H > 1.25$, u_N increases with H, but the height of the nose h_N decreases with H, as for the one-layer model case. For $H < 1.25$ ($1/H > 0.8$), approximately, the criticality $b_N = 1$ consideration inverts the trend of h_N vs. H, yet u_N remains an increasing function of H, as a result of the *Fr* correlation. When u_N is at the critical value, we also obtain $h_N/H = C$, and the value of the constant C is 0.347, 0.500, 0.427 and 0.428 for the *Fr* correlation B, RS, HS and UZ, respectively. Experimental results of u_N, taken from the paper of Rottman and Simpson [3], are also shown. There is fair agreement between theory and experiment, and, as already noted in previous studies, the Froude number relationship of Benjamin [6] over-predicts the speed of propagation. The best agreement is obtained with the correlation UZ suggested in this paper.

The numerical solutions of the two-layer SW equations are in excellent agreement with the analytical results of u_N and h_N during the slumping stage, and confirm the previous qualitative conclusions about the shape of the domain behind the nose. The numerical solutions also provide the details of the time-dependent behaviour of the current, and in particular the slumping distance x_s.

For example, the numerical results for the $H = 1$ case, using the HS *Fr* correlation, are presented in Fig. 9. In this case the nose moves with the critical $u_{N\max} = 0.43$ and leaves behind a downwardly-inclined interface. Initially, the interface in the

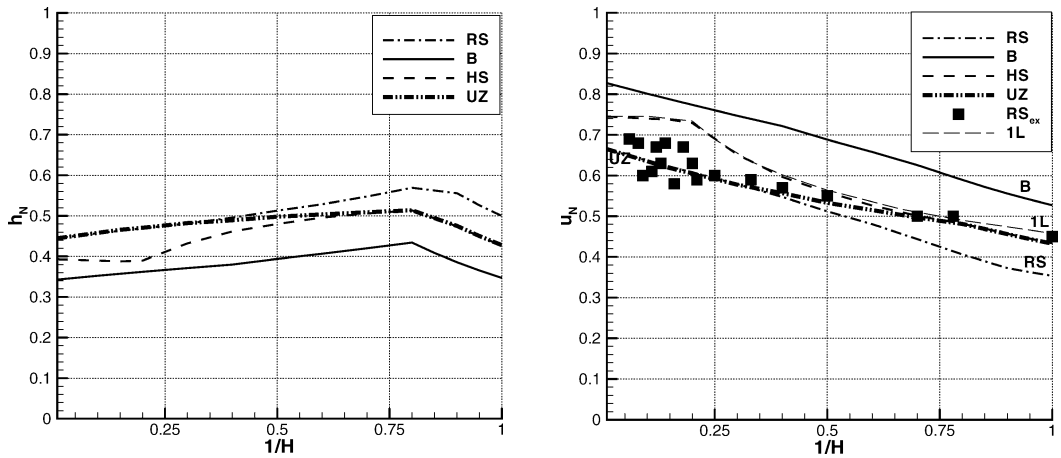

Fig. 8. Two-layer slumping results for h_N and u_N as functions of $1/H$ for various Fr correlations. Also shown for u_N: one-layer (1L) and experimental (symbols) results.

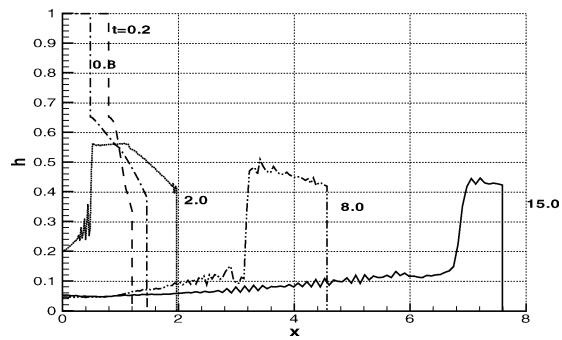

Fig. 9. Numerical SW two-layer results for case $H = 1.0$: $h(x)$ as a function of x at various times.

region $x < 1$ has a jump of $h_* = 0.35$ which moves to the left, until it reaches the end-wall $x = 0$ (at $t \approx 1.9$). The left-moving discontinuity is reflected from the wall as a right-moving bore, that produces a deep penetration of the upper fluid into the lower region. Subsequently, the bore propagates from the end-wall towards the nose which moves with its initial velocity and height. The bore arrives at the nose at time $t_s = 20.2$ and position $x_s = 9.8$; this stage is not schown in Fig. 9. (The oscillations in the profiles are a spurious numerical effect.)

A summary of slumping distance data, i.e., the length x_s of the gravity current when the front speed begins to decrease, is plotted in Fig. 10 as a function of $1/H$. The theoretical curves were obtained by the present numerical solution of the two-layer problem, and also shown is the solution of the one-layer problem (with the HS Froude correlation). The experimental results are from Rottman and Simpson [3] (Fig. 11). The available experimental points are quite scattered, and have been obtained indirectly from the plots of the recorded motion. In particular, for $H < 2$, x_s was marked by the intersection of the plotted bore and nose vs. time curves, see below; Rottman and Simpson remarked that this procedure is expected to over-estimate x_s. In any case, the accuracy of the experimental points is low and it is difficult to draw strong quantitative conclusions from this comparison.

The experimental results show that the length x_s increases from about 4.0 for $H = \infty$ to about 10.0 for $H = 1.0$, which is in fair agreement with the numerical computation for the two-layer case. The predictions of the one-layer model are qualitatively different with respect to the influence of H, yet the values of x_s are in acceptable agreement with the experiments for $H > 4$. The theoretical curves for the Froude relationship B seems to provide the best agreement with experiments, in particular for $H < 5$. However, the results of correlations HS and UZ can be considered in similar agreement, on account of the expected over-prediction of the experimental evaluation. Evidently, additional and more accurate experiments are needed for a better resolution of this issue.

Fig. 11 is a plot of the front and the bore position for the case $H = 1.0$ as functions of time after release. The theoretical curves show our numerical results for two correlations of Fr, and we also present the straight-line fits to the experimental data presented by Rottman and Simpson [3]. Initially, the front travels at constant speed until the bore, which propagates with

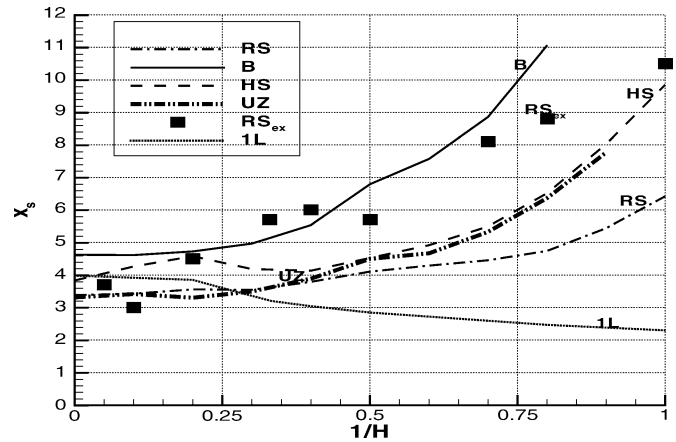

Fig. 10. Two- and one-layer slumping results for x_s as function of $1/H$ for various *Fr* correlations, and experimental points from Rottman and Simpson [3].

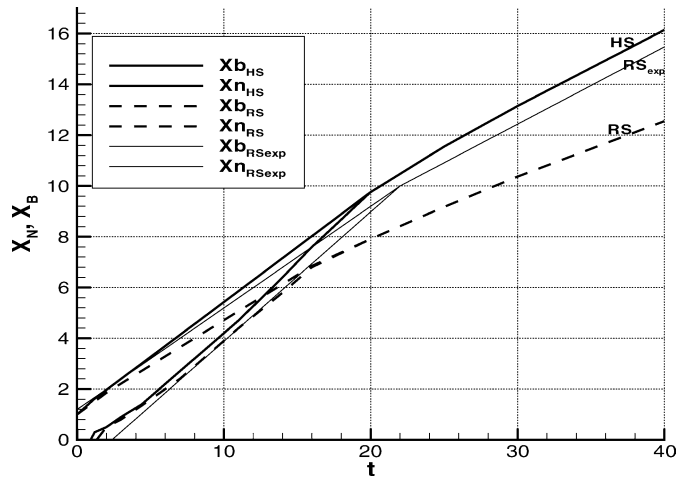

Fig. 11. Nose and bore positions as functions of time in configuration with $H = 1.0$. Numerical results for the *Fr* correlation HS and RS, and experimental curves from [3].

non-constant speed, reaches it (at the point where the two lines intersect) and then the front speed begins to decrease. The experimental (average) velocity of the bore is 0.55, while the initial V_b calculated analytically by (2.17), (2.18) is 0.51. The qualitative agreements between theory and experiment is excellent. Quantitatively, the HS *Fr* correlation yields better agreement that the RS correlation.

4. The axisymmetric case

The axisymmetric case is more intriguing than the 2D rectangular case from both theoretical and experimental aspects. The analysis is performed in a cylindrical coordinate system similar to the rectangular one with x replaced by the radial coordinate r. The analytical complication follows from the fact that now the SW equations (2.4) contain, in the RHS, the curvature source terms $-uh/r$ and $u^2h/[(H-h)r]$, respectively. The balance on the $\mathrm{d}r/\mathrm{d}t = c_\pm$ characteristics, see (2.7), becomes

$$\mathrm{d}h + M_\pm \,\mathrm{d}u = -\frac{uh}{r}\left(1 - M_\pm \frac{u}{H-h}\right)\mathrm{d}t, \tag{4.24}$$

where

$$M_\pm = \frac{-1}{1-b}\left[au \mp \sqrt{(au)^2 + (1-b)h}\,\right]. \tag{4.25}$$

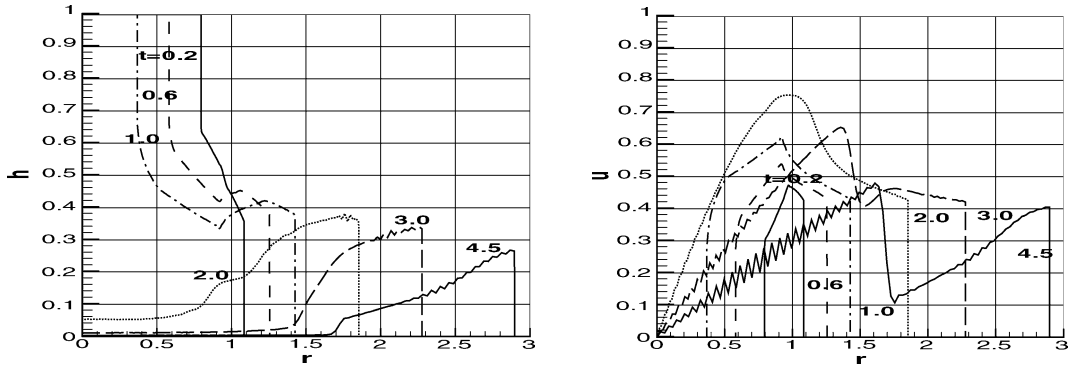

Fig. 12. Numerical SW two-layer results for axisymmetric case $H = 1.03$: h and u as functions of r at various times.

The source terms introduce time-dependencies which prevent formulation of analytical results of the type attained in the 2D case. The numerical solution, on the other hand, can be readily extended to this geometry. We argue that the left-moving jump conditions of the $H < 2$ case are not affected by the curvature terms, at least during the initial time period, because they reproduce a local balance. The differences between the 2D and axisymmetric case concerning the slumping behaviour are evaluated as follows.

The propagation at $t = 0^+$ starts with the same u_N and h_N as calculated for the 2D case because the contribution of the RHS of (4.24) is negligible for a very small time interval. Subsequently, in the 2D case the typical component of the slumping phase is a domain with constant h and u that trails the nose for at least $t = 5$. But the non-zero RHS term of (4.24) renders the region with constant h and u impossible for finite t. Along a c_+ characteristic which reaches the nose both h and u decrease, and hence a slumping stage of propagation with constant u_N is, typically, not possible. This prediction has been confirmed by numerical solutions of the SW equations for both the one- and two-layers models [18,19].

An interesting exception, however, is indicated by the two-layer model for H close to 1. In this case the critical constraint, $b_N = 1$, is expected to affect the motion. When this restriction is relevant the nose propagates with the constant $u = u_{N\max}$, see (2.14). In other words, this constraint overrides the tendency of the nose velocity to vary with time as long as the result would be propagation with supercritical speed. In this case the domain trailing the nose is mostly an expansion region with $b > 1$ covered by the c_- characteristics, like in the rectangular geometry counterpart. However, in the present cylindrical geometry the source terms in the righ-hand side of (4.24) reduce with time the velocity in the domain left behind the nose, and eventually suppress the possibility (or need) of propagation with $u_{N\max}$. Consequently, the motion with constant critical u_N can be sustained only for a short time interval ($t \approx 4$ for $H = 1$, at most). Afterwards, the nose is affected by the c_+ characteristics and both u_N and h_N decay with time. This behaviour is illustrated in Fig. 12 by numerical SW results for $H = 1.03$ (this value corresponds to an experiment considered later).

Our theoretical conclusion is that slumping with constant u_N and h_N in axisymmetric configuration is expected only for $H < 1.25$ (approximately) and even in this case it occurs over a short time period ($t < 4$) and distance ($r_N < 3$). The slumping decays due to propagation of small perturbations, in contrast to the prominent bore observed in the 2D case.

The experimental evidence concerning the slumping behaviour in axisymmetric geometries is problematic. We can say that, in general, it does not contradict the theoretical predictions, and provides some confirmation for the $H \approx 1$ case. Few truly axially symmetric configurations were tested, and most data referred to as "axisymmetric" was actually obtained in sector (wedge) tanks of about 10° to 20°. The influence of the side-walls of these tanks on the propagation is not known. A more severe restriction emerges from the viscous forces, which, following the arguments of [20], begin to dominate the inertial forces when

$$r_N > r_V = (Re\, h_0/r_0)^{1/6}, \tag{4.26}$$

where $Re = Uh_0/\nu$. (In the rectangular counterpart the right-hand side contains the less restrictive power 2/7.) For the typical $Re = 10^4$ and $h_0/r_0 = 0.1$, we obtain the very restrictive $r_V = 3.2$. Simpson [21] analyzed self-performed laboratory tests with saline in wedges of 10° and 20° (and also some Thorney Island test that concern non-Boussinesq fluids and are irrelevant to our discussion). The $(r_N - 1)$ vs. t points were plotted on log–log axes, and straight lines with slopes 1 and 1/2 were fitted to the initial and final points to represent the expected asymptotes of spread with t and $t^{1/2}$. The "length of constant speed" was defined as the radial position where these lines intersect, and the so obtained values of r varied from 5 to 3 as H varied from 1 to ∞. However, a careful examination of these plots, as well as of additional experiments [22,23] shows that the outcome of this graphic procedure is not a slumping distance in accordance with our definition. With the exception of the $H = 1$ results, some variations of u_N in the initial stage are observed, and the deviation from the line with slope 1 starts a considerable

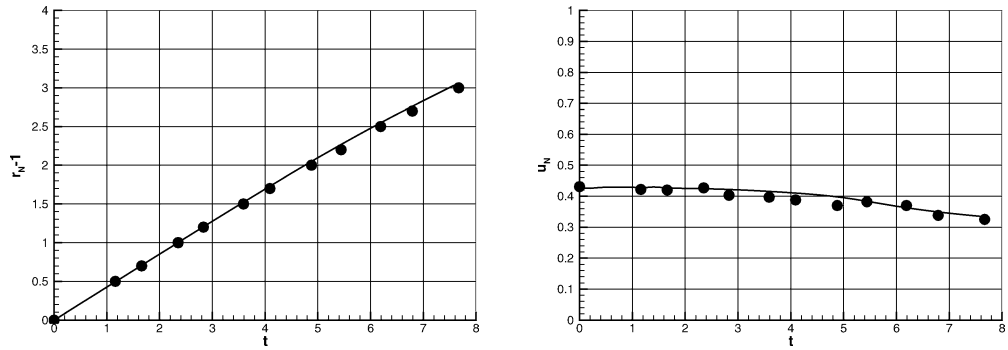

Fig. 13. Axisymmetric current with $H = 1.03$: distance of propagation and velocity of nose as functions of time, experiments (dots) and SW (lines) results.

distance before the point of intersection of the asymptotes. The log–log plots used by [21] are, in our opinion, not a sufficiently accurate tool for drawing clear-cut conclusions about the slumping. Moreover, the employed experimental data was prone to viscous influence (typically, $r_V \approx 4$) and hence the transition to the $1/2$ slope asymptote is unreliable. Only the set labeled R of Simpson [21], for $H = 1$, yields, quite convincingly, the initial constant $u_N = 0.40$ for $r < 4$. The present calculations show that in this case the nose moves with the constrained velocity 0.43 for about $r_s = 3$. The agreement is fair, and the discrepancies can be attributed to experimental and numerical errors.

Fig. 13 shows a comparison of our numerical solution with a genuine axisymmetric experiment performed in a large cylindrical tank at the Coriolis Laboratory in Grenoble (see Hallworth et al. [23], Table 1, Expt S2; in this case $r_V \approx 7$). (More details of the SW solution are given in the previous figure.) The excellent agreement of $r_N(t)$ between experiment and theory lends support to our analysis, but a larger body of data is needed for a final confirmation. Fig. 13 illustrates how difficult it is to determine accurately the end of the slumping stage from a plot of r_N vs. t: the impression is that the slope is constant for $t \approx 7$, but the more detailed Fig. 12, as well as a plot of u_N vs. t, indicate a decrease of speed for $t > 4$.

5. Box model revisited

Box models provide quick momentum-integral type approximations to the motion of the gravity current. Since they are still widely used, it is proper to briefly discuss their ability to reproduce the slumping stage. Moreover, this model is of historical importance to our problem, because it was the main means in the pioneering attempts of Huppert and Simpson [2] to understand the slumping behaviour and develop the practical Fr correlation HS. However, a re-examination of that theory in view of the present results shows that the suggested interpretation of the slumping effects by means of a box model is not acceptable.

Huppert and Simpson [2] modeled the current as a rectangular box subject to volume continuity and governed by the nose motion relationships (2.9) and (2.12). In the present scaling this can be formulated as

$$h_N(t) = \frac{1}{x_N(t)}, \tag{5.27}$$

$$u_N = \frac{\mathrm{d}x_N}{\mathrm{d}t} = Fr\, h_N^{1/2}, \tag{5.28}$$

with Fr given by (2.12), and subject to $x_N(t = 0) = 1$. The special form of (2.12) is essential for the interpretation suggested by the authors, namely, that the slumping stage corresponds to the spread of the current from its initial $h_N = 1$ to the position where $h_N = 0.075H$. In this range $Fr \propto h_N^{-1/3}$, and hence $u_N \propto h_N^{1/6}$. This slow variation of u_N emulates a constant velocity behaviour. This is in contrast with the subsequent behaviour, $u_N = 1.19h_N^{1/2}$, in the post-slumping stage for $h_N < 0.075H$.

There are several implausible points in this interpretation. First, for a deep ambient $H > 13.33$ the model predicts no slumping stage at all, i.e., $x_s = 1$ and $t_s = 0$. The present SW results, as well as experiments, indicate the appearance of a short, but clear-cut slumping stage ($x_s \approx 4$ and $t_s \approx 5$) for large H. Second, the velocity u_N predicted by the model is not truly constant. For $H = 1$, for example, the box-model u_N varies during the slumping stage from 0.50 to 0.32, i.e., a decrease of 35% as h_N decreases from 1 to 0.075. The two-layer SW approximation, with the same Fr correlation, predicts the constant $u_N = 0.43$ during the slumping stage. Third, the model of Huppert and Simpson [2] is reliant on the particular Fr correlation (2.12) which received no theoretical backing since it has been postulated about twenty years ago. In contrast, we show here that the SW formulations yield a clear-cut slumping stage for various plausible continuous Fr correlations with h_N/H, including

the classical theoretical formula of Benjamin [6]. The conclusion is that the box-model description of the slumping behaviour is erroneous, both qualitatively and quantitatively. With hindsight, this is not surprising: the slumping behaviour is dominated by the arrangement and backward–forward propagation of perturbations on characteristics in a combined initial and boundary value problem, while the box model is a simplified initial-value approximation.

What is nevertheless remarkable about the box-model is its ability to predict, with tolerable error (say, up to about 10%), the distance of propagation $x_N(t)$ for quite long times after the release. The reasons are as follows. (1) In the box-model, in contrast to the SW results, the nose height decays continuously with time from $h_N = 1$, and hence the motion first overtakes, then lays behind the real velocity of propagation. The discrepancies in the integral $x_N(t)$ are therefore not as large as could be anticipated from the maximal differences in the velocity prediction. (2) After the decay of the slumping phase a gravity current (in a deep ambient) attends a self-similarity behaviour in which the propagation is governed mainly by the total volume, see [24], in close resemblance with the assumption of the box model. In view of these observations, it makes sense to use this model as a guiding approximation of the propagation, but, again, not for the understanding of the slumping motion.

The advantage of the correlation (2.13) in box-model calculations of $x_N(t)$ is now illustrated. Substitution of this equation and (5.27) into (5.28) yields an expression for $\mathrm{d}x_N/\mathrm{d}t$ which is easily integrated. After some arrangement and use of $x_N(0) = 1$, we obtain

$$x_N(t) = \left[\left(1 + \frac{3}{H}\right)^{3/2} + \frac{3}{2}t\right]^{2/3} - \frac{3}{H}. \tag{5.29}$$

The axisymmetric counterpart yields a more complex, but still convenient, result

$$t = \int_1^{r_N} \left(r^2 + \frac{3}{H}\right)^{1/2} \mathrm{d}r = I(r_N) - I(1), \tag{5.30}$$

where

$$I(r) = \frac{1}{2}\left[r\left(r^2 + \frac{3}{H}\right)^{1/2} + \frac{3}{H}\ln\left(r + \left(r^2 + \frac{3}{H}\right)^{1/2}\right)\right]. \tag{5.31}$$

6. Concluding remarks

The slumping behaviour of a gravity current has been analysed in the framework of the two-layer SW formulation. Novel theoretical insights have been obtained (some in contradiction with previous beliefs). In particular, the $H < 2$ (shallow-ambient) and axisymmetric configurations were resolved.

We showed that for all values of H and plausible nose Froude correlations, a rectangular gravity current of fixed volume, which is released from behind a lock, displays an initial stage of propagation with constant velocity u_N and nose-height h_N. The slumping distance x_s increases from about 4 to 10 as H decreases from ∞ to 1 (the most dramatic increase, from about 5 to 10, occurs in the domain $H < 2$). This special behaviour prevails during the period when the initial depression wave generated at the lock travels back to the end-wall, and then, after reflection, travels forward and reaches the nose. Thus, the slumping behaviour is expected to be an important ingredient of the practical lock-release problem, and provides a stringent criterion for comparisons and validation of data.

The one-layer SW model approximates well the value of x_s for large H, but mispredicts the dependency of x_s on H.

The flow-field in the shallow-ambient case, $H < 2$, is more complicated and interesting than the deep-ambient counterpart. First, a backward moving discontinuity of the interface for $H < 2$, and an expansion region behind the constrained-nose for $H < 1.25$ (approximately), show up. Second, a forward-moving bore is created by the reflection of that discontinuity. These features have been accounted for in the present analysis of the slumping behaviour, and thus we closed the $1 \leqslant H < 2$ gap left open by the previous theoretical investigations. We showed that the velocity of the reflected bore increases significantly when H varies from 1 to 2 and therefore the slumping distance decreases strongly upon this change of H. The numerical solver of the SW equations was specially designed to treat the left-moving discontinuity as a moving-boundary condition.

We compared four different nose Froude correlations. We showed that the qualitative behaviour of the slumping stage is not affected by the particular choice. Compared with experiments, the *Fr* relationship B provides the best fit for x_s, but correlations RS and HS yield the best agreement of u_N for small and large H, respectively. The new correlation UZ, introduced here as an ad-hoc simple compromise between previous suggestions, seems to provide a fair combination of these agreements, as well as improved simplicity of use in box-model approximations.

We showed that a cylindrical axisymmetric gravity current is qualitatively different from the rectangular 2D counterpart with respect to a slumping stage with constant u_N and h_N. Typically, such a stage does not exist because the curvature effects enforce

a monotonic decrease of u_N and h_N. The exception is the constrained $u_{N\max}$ nose velocity case that appears for $H < 1.25$ (approximately), and even in these circumstances the slumping distance and time are considerably shorter and their decay is smoother than in the 2D counterpart.

The present results are in good agreement with the experimental observations of Rottman and Simpson [3]. This gives credence to the SW two-layer formulation. The numerical results of the SW equations are in excellent agreement with the analytical results that can be obtained for some of the dependent variables. This comparison provides credence to the numerical methods employed here, as well as useful simplifications and interpretations of the computed behaviour. However, the jump conditions used in the configurations with $H < 2$ are not unique, and different hypotheses may provide improved results; this topic is left for future investigation along the lines of [16] and [17].

The present analysis indicates that currents released in non-deep ambient (say, $H < 3$) must be treated with care because they may display some a-typical intrinsic features, and, in particular, significant slumping distances. This warning has practical aspects. The experimental investigations tend to concentrate in the domain of $H < 2$ because of the practical dimensions of laboratory equipment (e.g., for $h_0 = 50$ cm and $H = 10$ an impractical tank of 5 m height is needed). On the other hand, the theoretical studies prefer the domain of large H because of the relative simplicity of the one-layer model. It turns out that, unfortunately, comparisons between results obtained in these different domains may be difficult, even misleading. The major question should be if the slumping distance and time may play a role in the compared variables. This warning also applies to the use of one-layer SW models, which distort the slumping, for simulation of non-deep currents. We hope that the detailed information provided in this paper will facilitate the wider use of two-layer model simulations in the gravity current research.

Finally, we remark that very few experiments have been dedicated to the slumping behaviour. With the progress in theory and in experimental techniques, new experiments are bound to throw additional useful light on this feature. This is especially relevant to the axisymmetric configurations and to the verification of the closure conditions for the jumps in the configurations with $H < 2$.

Acknowledgements

MU wishes to thank Prof. H.E. Huppert for stimulating discussions on gravity currents, and Dr. J.E. Simpson for providing experimental data on axisymmetric currents. The research was partially supported by the Fund for the Promotion of Research at the Technion and by the Bar-Nir Bergreen Software Technology Center of Excellence.

Appendix A. Numerical solutions of the SW equations

Some details of the numerical solution of the two-layer model are presented.

Following the approach of [7], we performed the numerical solution using a finite difference, two-step Lax–Wendroff method [25,26].

We distinguish between the $H < 2$ and $H > 2$ cases. In the former case, it is necessary to solve differently two phases of propagation: the first one extends from $t = 0$ until the left-moving jump, see Fig. 2, reaches the left wall, $x = 0$; the domain of solution is $x_f(t) \leqslant x \leqslant x_N(t)$. During the second phase the domain of solution is $0 \leqslant x \leqslant x_N(t)$. In case $H > 2$ no jump is expected, therefore the first phase is not needed.

A.1. The first phase for $H < 2$

In the fluid domain to the left of the jump, $0 \leqslant x \leqslant x_f(t)$, the initial conditions $u(x) = 0$, $h(x) = 1$ are preserved. The numerical solution is needed in the physical domain $x_f(t) \leqslant x \leqslant x_N(t)$.

It is convenient to keep the current in a constant computational domain, therefore the x-coordinate was mapped into

$$y = \frac{x - x_f}{x_N - x_f}, \tag{A.1}$$

where $0 \leqslant y \leqslant 1$. Consequently, the original equations (2.4) were subjected to the following transformations:

$$\begin{aligned} \left(\frac{\partial}{\partial t}\right)_x &= \left(\frac{\partial}{\partial t}\right)_y - \frac{\dot{x}_f + y(\dot{x}_N - \dot{x}_f)}{x_N - x_f} \cdot \left(\frac{\partial}{\partial y}\right)_t, \\ \left(\frac{\partial}{\partial x}\right)_t &= \frac{1}{x_N - x_f} \cdot \left(\frac{\partial}{\partial y}\right)_t \end{aligned} \tag{A.2}$$

and in the conservation form, they are expressed as:

$$\begin{cases} \dfrac{\partial h}{\partial t} = \dfrac{1}{x_N - x_f}\left[Y\dfrac{\partial h}{\partial y} - \dfrac{\partial q}{\partial y}\right], \\ \dfrac{\partial q}{\partial t} = \dfrac{1}{x_N - x_f}\left[\left(Y - \dfrac{q}{h}(2-2a)\right)\dfrac{\partial q}{\partial y} + \left((1-2a)\dfrac{q^2}{h^2} - h(1-b)\right)\dfrac{\partial h}{\partial y}\right], \end{cases} \tag{A.3}$$

where $q = u \cdot h$, the upper dot denotes time derivative, and

$$Y = \dot{x}_f(t) + y\big(\dot{x}_N(t) - \dot{x}_f(t)\big). \tag{A.4}$$

The left-side boundary condition are provided by the jump, see Section 2.4.1,

$$\begin{cases} u(y=0) = \dot{x}_f = \dfrac{V_f h_*}{1-h_*}, \\ h(y=0) = 1 - h_*. \end{cases} \tag{A.5}$$

The boundary conditions for h at $y = 1$ must be calculated for each new time step from the balances on the characteristic c_+ which reaches the nose. This is actually combined with the calculation of u_N by (2.9) and subject to the criticality constraint (2.14).

The equations were discretized on a grid with constant Δy intervals (the corresponding Δx follows from (A.1)). Typically, the number of intervals was 100–200, and the ratio of the time step to Δy was 0.1–0.2 (since the typical velocities in the system are smaller than 1, the resulting effective Courant number is significantly below the necessary stability restriction, see [25]).

A small artificial viscosity term, $\sim \beta \Delta x \partial^2 q/\partial x^2$ (see details in [7], Appendix A) was added to the RHS of the momentum equation to dampen spurious numerical oscillations. The coefficient β was typically 0.1–0.2.

For $H < 2$, for numerical convenience (elimination of steep initial gradients), we initialize the positions of the nose and jump at (approximately) $x = 1 \pm 0.1$ and assume linear variation of h and u between the corresponding boundary conditions. (We assume that at $t = 0$ the system already contains the jump.)

A.2. The second phase

In this phase no jump at the interface is present and therefore $x_f(t)$ and V_f are equal to zero. As before, the coordinate transformation (A.1) is used to solve the original system of equations. The boundary conditions at the nose are identical to these of the first phase, but at $x = y = 0$ we impose $u = 0$ and determine the time-dependent $h(y = 0)$ from the balance on the c_- characteristic.

In the ideal situation there is no difficulty to switch from the first to the second phase of propagation by a simple change of the boundary conditions at $y = 0$. In real computations, however, some matching was necessary. When the jump arrives to the left boundary the velocity $u(y = 0)$ different from zero and, if this value is changed abruptly to satisfy the subsequent boundary conditions, the numerical solution becomes unstable. This actually indicates a physical problem: the shallow-water inviscid equations are not valid in the small region and time interval where the jump is stopped by the boundary and then reflected as a bore, see Section 2.4.2. To overcome this instability, we stop artificially the first phase slightly earlier than above, when the distance of the jump from the left boundary wall is small (typically, $x_f \approx 0.1$). This is expected to introduce a small error in the results, but stabilizes the solution. The good agreement between the numerical and analytically approximated reflected bore results provide support to this smoothing method.

We would like to mention that the incorporation of the "first phase" in the shallow-water solution of the gravity current released from behind a lock is, to our best knowledge, a new contribution. When $H > 2$ the first phase and the matching are obviously not needed, and the solutions starts straightforwardly from the "second" phase with initial conditions $h = 1$ and $u = 0$ in $0 \leqslant x \leqslant 1$.

A.3. Validation

The numerical solver has been subject to various tests of accuracy and convergence, in particular: (1) We performed comparisons with the analytical results when available, such as: the values of u_N and h_N, the backward propagation of the depression wave (for $H > 2$), the behaviour in the $H \gg 1$ limit. (2) We performed comparisons with the numerical results of [3] (obtained by a different numerical scheme based on the method of characteristics), for compatible configurations. (3) We checked convergence using various grids (100–400 intervals), time steps and artificial viscosity coefficients. In topics (1) and (2) we obtained perfect agreements. In topic (3), we found that, typically for $H \geqslant 1.25$, the profile of $x_N(t)$ during the slumping phase varied by less than 1% due to that variation of the numerical parameters. The artificial viscosity (with coefficient $\beta = 0.1$–0.2) reduced significantly the spurious oscillations of h and u (to typically 1–3%) without any observable (in the plots of (A.4) size used for comparisons) contribution to the mean profiles of h, u, or velocity or propagation.

The results are less robust for $H \approx 1$, and some trial and error in the choice of the numerical parameters was necessary to avoid instability. For example, in the run for Fig. 9 we used a numerical grid of 100 points with a time step of 2×10^{-3} and artificial viscosity coefficient $\beta = 0.12$. With other tested values of β the numerical computations stopped before the end of the slumping stage because accumulated numerical errors produced the "impossible" situation of $u - c_+ < 0$ near the nose (note that a small numerical error may easily change the sign of this difference in a region where u and c_+ are very close). The numerical difficulties encountered when H becomes close to 1 can be attributed to the fact that the mathematical problem is expected to be ill-conditioned in this domain of critical nose velocity; one of the eigenvectors of the matrix of coefficients of the hyperbolic system becomes singular and loss of significant digits may occur. We checked carefully our results in these more problematic cases and we estimate that the numerical errors in $x_N(t)$ are also about 1–2%. We think that this numerical error is acceptable because: (1) This is in the range of the intrinsic inaccuracies of the inviscid shallow-water model (e.g., the Boussinesq approximation, the neglected friction on the solid boundary, etc.). (2) The errors in the experimental data which we used for comparison is also estimated to be several percent. (3) The insights and conclusions reported in this paper will certainly remain unchanged by an increased numerical accuracy.

Appendix B. Approximations for jump conditions

For convenience of use, the jump condition results are also presented by the fitted polynomial approximations

$$V_f \approx 0.1798H + 0.3475 \quad (1 \leqslant H \leqslant 2) \tag{B.1}$$

and

$$h_* \approx -0.093H^2 - 0.066H + 0.507 \quad (1 \leqslant H \leqslant 2). \tag{B.2}$$

The position of the jump is simply

$$x_f(t) = 1 - V_f t \approx 1 - (0.1798H + 0.3475)t. \tag{B.3}$$

References

[1] G.H. Keulegan, An experimental study of the motion of saline water from locks into fresh water channels, Technical Report 5168, Natl. Bur. Stand., 1957.
[2] H.E. Huppert, J.E. Simpson, The slumping of gravity currents, J. Fluid Mech. 99 (1980) 785–799.
[3] J. Rottman, J. Simpson, Gravity currents produced by instantaneous release of a heavy fluid in a rectangular channel, J. Fluid Mech. 135 (1983) 95–110.
[4] T. Maxworthy, J. Leilich, J.E. Simpson, E.H. Meiburg, The propagation of gravity currents in a linearly stratified fluid, J. Fluid Mech. 453 (2002) 371–394.
[5] J.B. Klemp, R. Rotunno, W.C. Skamarock, On the dynamics of gravity currents in a channel, J. Fluid Mech. 269 (1994) 169–198.
[6] T.B. Benjamin, Gravity currents and related phenomena, J. Fluid Mech. 31 (1968) 209–248.
[7] R.T. Bonnecaze, H.E. Huppert, J.R. Lister, Particle-driven gravity currents, J. Fluid Mech. 250 (1993) 339–369.
[8] S.J.D. D'Alessio, T.B. Moodie, J.P. Pascal, G.E. Swaters, Gravity currents produced by sudden release of a fixed volume of heavy fluid, Stud. Appl. Math. 96 (1996) 359–385.
[9] M. Ungarish, H.E. Huppert, On gravity currents propagating at the base of a stratified ambient, J. Fluid Mech. 458 (2002) 283–301.
[10] A.J. Hogg, M. Ungarish, H.E. Huppert, Effects of particle sedimentation and rotation on axisymmetric gravity currents, Phys. Fluids 13 (2001) 3687–3698.
[11] M.A. Hallworth, H.E. Huppert, J.C. Phillips, R.S.J. Sparks, Entrainment into two-dimensional and axisymmetric turbulent gravity currents, J. Fluid Mech. 308 (1996) 289–311.
[12] C. Härtel, E. Meiburg, F. Necker, Analysis and direct numerical simulation of the flow at a gravity current head. Part 1. Flow topology and front speed, J. Fluid Mech. 818 (2000) 189–212.
[13] Stommell, Farmer, Abrupt change in width in two-layer open channel flow, J. Mar. Res 11 (1952) 205–214.
[14] J. Billingham, A.C. King, Wave Motion, Cambridge University Press, 2000.
[15] P.G. Baines, Topographic Effects in Stratified Flows, Cambridge University Press, 1995.
[16] J.B. Klemp, R. Rotunno, W.C. Skamarock, On the propagation of internal bores, J. Fluid Mech. 331 (1997) 81–106.
[17] J.R. Wood, J. Simpson, Jumps in layered miscible fluids, J. Fluid Mech. 140 (1983) 329–342.
[18] M. Ungarish, T. Zemach, On axisymmetric rotating gravity currents: two-layer shallow-water and numerical solutions, J. Fluid Mech. 481 (2003) 37–66.
[19] M.A. Hallworth, H.E. Huppert, M. Ungarish, On inwardly propagating axisymmetric gravity currents, J. Fluid Mech. 494 (2003) 255–274.

[20] H.E. Huppert, The propagation of two-dimensional and axisymmetric viscous gravity currents over a rigid horizontal surface, J. Fluid Mech. 121 (1982) 43–58.
[21] J.E. Simpson, Axisymmertic gravity releases, Private communication, 2002.
[22] P. Huq, The role of aspect ratio on entrainment rates of instantaneous, axisymmetric finite volume releases of dense fluid, J. Hazardous Materials 49 (1996) 89–101.
[23] M.A. Hallworth, H.E. Huppert, M. Ungarish, Axisymmetric gravity currents in a rotating system: experimental and numerical investigations, J. Fluid Mech. 447 (2001) 1–29.
[24] R.E. Grundy, J. Rottman, The approach to self-similarity of the solutions of the shallow-water equations representing gravity current releases, J. Fluid Mech. 156 (1985) 39–53.
[25] K.W. Morton, D.F. Mayers, Numerical Solutions of Partial Differential Equations, Cambridge University Press, 1994.
[26] W.H. Press, S.A. Teukolski, W.T. Vetterling, B.P. Flannery, Numerical Recipes in Fortran, Cambridge University Press, 1992.